Raman scattering and phonon dispersion in Si and GaP at very high pressure

Bernard A. Weinstein*† and G. J. Piermarini
Institute for Materials Research, National Bureau of Standards, Washington, D. C. 20234
(Received 16 January 1975)

One- and two-phonon Raman spectra of Si and GaP were measured at room temperature for pressures up to 135 kbar. An opposed diamond-anvil high-pressure cell was employed in the experiments, and its design and use for Raman scattering are described in detail. Mode Grüneisen parameters and quadratic pressure coefficients were measured for phonons at several zone-boundary critical points as well as at $\vec{q} \approx 0$. In addition the general effect of pressure on large portions of the phonon dispersion near the zone edge could be inferred. In both materials zone-boundary TA modes "softened" with increasing pressure, while optical phonons shifted to higher energy. Using the high-pressure Raman data a calculation of the thermal-expansion coefficient of Si as a function of temperature (negative at low temperature) achieved fair agreement with experiment. Measured and theoretically calculated mode Grüneisen parameters are compared for several tetrahedral semiconductors. The Raman spectrum of Si was measured up to the metallic (β-Sn structure) tansformation at 125 ± 5 kbar. This transition is discussed within the context of the bond-charge model.

INTRODUCTION

Raman scattering at very high pressure offers many attractions as a means for investigating phonon properties of solids. First, anharmonic effects may be studied for comparatively large volume changes. For example in Si, a pressure of 100 kbar[1] produces a volume decrease of roughly 5%,[2] whereas the total volume change for this material in going from absolute zero to its melting temperature is only ~1.8%.[3] Furthermore, the influence of temperature is complicated by statistical effects, but hydrostatic pressure manifests itself only through volume change. Second, the volume dependence of the phonon dispersion can be used as a rather stringent test of various lattice-dynamical theories, as it is difficult to correctly calculate both the dispersion and the mode-Grüneisen parameters without a realistic description of both long- and short-range crystal forces. Experimentally, we find that 100-kbar pressures produce large phonon-frequency shifts which can be measured accurately even for the second-order Raman spectrum. In addition, nearly degenerate (or accidentally degenerate) critical points may separate and become easily identifiable at large hydrostatic pressures.

Finally, many different phase transformations, which can be induced at high pressure, may be readily studied by Raman scattering. For example, the volume dependence of "soft" modes associated with ferroelectric and other transitions may be investigated.[4,5] Where structural changes occur, considerable information concerning the symmetry of the various phases can be obtained by measuring polarized Raman spectra. Of particular interest to this work is the first-order semiconductor-to-metal transition occurring in Si and other tetrahedral semiconductors.[6]

Several Raman-scattering investigations of crystals under pressure have been reported. Notable among these are the works of Mitra *et al.*[7-9] on transparent semiconductors and other materials, and Cardona *et al.*[10-12] on opaque semiconductors. In these experiments hydrostatic pressure up to 10 kbar was produced hydraulically inside an oil-filled optical cell.[9] Several Raman studies using uniaxial stress have also been performed[13,14]; in these the maximum pressure was usually limited to $\lesssim$25 kbar by sample breakage. Although a great deal of useful information was obtained from the above experiments, the relatively low pressure often made it difficult to accurately measure the resulting small phonon-frequency shifts, and a host of phase transitions occurring at higher pressure could not be studied.

Early use of the diamond-anvil cell in conjunction with Raman scattering by the groups of Lippincott[15] and Mitra[16] met with only limited success. More recently, Adams *et al.*[17] used an ungasketed diamond-anvil cell in Raman measurements up to 40 kbar, and Cerdeira *et al.*[18] employed a gasketed sapphire-anvil cell which on occasion has produced hydrostatic pressure up to 80 kbar before the sapphire-anvil shattered. Our experiments with GaP (Ref. 19) and Si have employed a gasketed diamond-anvil cell which is capable of achieving 100-kbar true hydrostatic pressure and 200 kbar in a quasihydrostatic-pressure environment.

Our aims in this publication are to describe in detail this pressure cell and its use for Raman-scattering experiments, and to present, discuss, and compare our measurements of the first- and second-order spectra of GaP and Si up to ~135 kbar. From the high-pressure Raman data we calculate the thermal-expansion coefficient of Si as a function of temperature and compare the result with direct measurements of this quantity. A

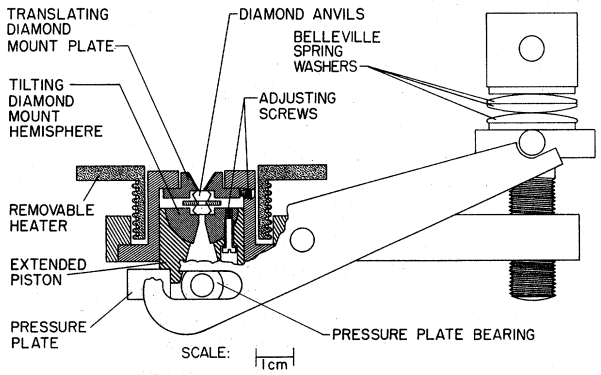

FIG. 1. Cut-away cross-section drawing of the Waspaloy-opposed diamond-anvil high-pressure cell used in this work. The removable heater was not employed in our experiments.

comparison of observed and theoretically predicted values of the mode-Grüneisen parameters of some tetrahedral semiconductors is also presented. Finally, we discuss the transformation to a highly opaque phase observed for Si at ~125 kbar. We believe this to be a semiconductor-to-metal phase transition. To the authors's knowledge these are the first detailed Raman investigations of phonon dispersion at such high pressure.

EXPERIMENT

Detailed descriptions of several types of NBS diamond-anvil high-pressure cells have been published. These cells are designed for specific applications such as x-ray diffraction (powders,[20] and single crystals[21]), optical microscopy,[22] and infrared spectroscopy.[21] Of particular interest to this paper is the recently published description of a Waspaloy diamond pressure cell designed for both high-pressure (200 kbar) and high-temperature (700 °C) capability.[23] A modification of this Waspaloy cell which incorporates design features that enhance its utility as an optical cell for Raman scattering measurements is used in the present study, and was also employed in a previous work which did not include a detailed description of the device.[19] The difference between the cell described here and the cell reported in Ref. 23 is the conical aperture of the diamond window which has been increased from 30° to 60° (see Fig. 1). The enlarged opening increases the amount of scattered light which can be effectively collected.

The essential components of the Waspaloy pressure cell for Raman-scattering studies are depicted in the cutaway cross-section drawing shown in Fig. 1. The principle employed to generate force is a spring-loaded lever-arm assembly. Force is produced by compressing Belleville spring washers with 272-kg capacity by the rotation of a screw. This arrangement produces a uniform and continuously changing force as the screw is rotated—a feature which has proved in practice to be highly desirable. These Belleville spring washers are used either in series or parallel to alter sensitivity and load characteristics as desired. The applied load is magnified by a factor of 2 on being transmitted through the lever-arm assembly to the pressure plate which is in contact with the extended piston containing one of the diamond anvils. The opposing anvil is fixed in position and acts as an entablature against which the piston anvil pushes.

Each anvil is a brilliant-cut gem (approximate size, $\frac{1}{3}$ carat) with the culet removed by grinding and polishing to form an irregular octagonal flat about 0.5 mm^2 in area. The usual distance between opposite sides of the octagon is between 0.6 and 0.8 mm. The regular octagonal surface parallel to this anvil flat, called the table, is approximately 3.5 mm between opposite sides (equal to an area of about 8 mm^2). The table is supported by a translating diamond-mount plate for the fixed anvil or entablature and a tilting diamond-mount hemisphere for the moving piston anvil; both types of motion are needed to accurately align the anvil faces.

The anvils are always used in the gasketed configuration as shown in Figs. 1 and 2. The metal gasket (Inconel X750) allows the sample to be encapsulated in a fluid-pressure–transmitting medium, thus providing a truly hydrostatic environment. The pressurized volume is defined by a gasket hole 0.5 mm in diameter and 0.15 mm thick. The sample, contained in this pressurized volume, is surrounded by a 4:1 mixture (by volume) of methanol: ethanol) which produces a hydrostatic environment to just over 100 kbar.[24] Because an increase in pressure is accompanied always by a volume decrease, the metal gasket must flow either by decreasing its diameter, its thickness, or both to achieve a smaller volume.

To measure pressure in the diamond cell, we use an optical-fluorescence system developed in our laboratory.[23] The system utilizes the pressure-dependent shift of the R_1 fluorescence line in ruby which has been calibrated recently to 200 kbar against the compression of NaCl. Pressures are based on Decker's equation of state for NaCl.[25]

In practice a small fragment of crystalline ruby (0.5% Cr by weight) is placed in the cell along with the sample and the methanol: ethanol pressure-transmitting fluid. The ruby fragment occupies about 10% of the pressurized volume and is usually sufficiently small as not to interfere with the desired measurement. In these experiments the pressure was measured *in situ* using the same laser light and monochromator system to excite and ana-

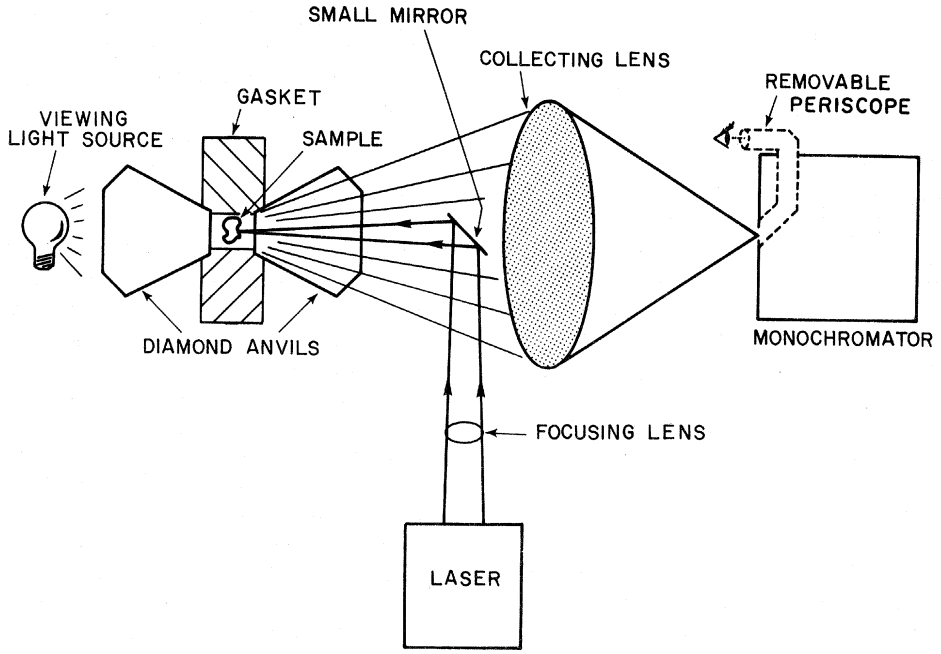

FIG. 2. Schematic diagram of the back-scattering experimental configuration used for high-pressure Raman-scattering measurements with the diamond-anvil cell. The figure is not drawn to scale.

lyze the ruby fluorescence as was used to measure the Raman scattering. For ambient conditions the R_1 line in ruby occurs at 6942 Å, and the second component of the doublet R spectrum, R_2, occurs at 6928 Å. At 25 °C, the pressure dependence of the R_1-peak position is linear to 200 kbar (in both wavelength and frequency within 0.6% standard deviation) with a shift of 0.365 Å/kbar or -0.753 cm^{-1}/kbar. At 100-kbar pressures are considered accurate to within ± 3%.

Use of the diamond-anvil cell in Raman-scattering experiments presents some particular difficulties which must be overcome. Earlier workers encountered four major problems.[15,16] They could not measure the pressure accurately, their ungasketed systems were not hydrostatic, only very thin samples ($\lesssim 1$ μm) of high scattering power could be studied, and the technique of forward scattering produced an intense background especially near the Rayleigh line. In the present work the first three of these problems have been eliminated. The pressure can be measured accurately and conveniently using the calibrated shift of the ruby R-line fluorescence. Introduction of a gasket between the diamonds allows hydrostatic conditions to be maintained up to ~100 kbar. The environment in the cell is then quasihydrostatic, but at the maximum pressure in these experiments, ~135 kbar, the magnitude of the stress gradients (as gauged by the slight broadening of the $R_1 - R_2$ ruby fluorescence doublet) remained small.[26] Also, the gasket, which at maximum pressure can still be 75–100 μm thick, permits one to study samples of reasonable dimensions. The problem of background radiation remains, but by using the equipment and techniques which are presently available, the background intensity can be reduced to a tolerable level.

Although one typically finds that the Raman intensity from a sample within the diamond cell has decreased by only a factor of 2 or 3 from that of the same sample outside the cell, the background radiation can increase by several orders of magnitude (depending on experimental conditions) when a cell is used. The background has several origins. Close to the frequency of laser excitation one must cope with an intense Rayleigh tail which results from spurious scattering by components of the cell in the vicinity of the sample (e.g., sample, liquid, ruby, gasket). Because of its design the diamond cell is only suited for the forward- or backward-scattering geometries, and of the two we have found that the latter results in less background radiation especially close to the laser frequency. Of course when studying opaque crystals (such as Si) the backscattering geometry must be used. A triple monochromator may be effectively employed to suppress the intense Rayleigh tail. However, use of an iodine prefilter is hampered by the high level of fluorescence usually excited from impurities in the diamond anvils by the 5145-Å Ar^+ laser line.

The experimental configuration employed in this work is drawn schematically in Fig. 2. The small mirror which reflects the incident light into the cell, also serves to intercept reflected and ~180° back-scattered light. Often signal-to-background ratio can be improved by blocking a larger portion of the central collection aperture. With a double monochromator, and the backward-scattering geometry, we have found that even under optimum conditions, it was difficult to measure spectra of intensity comparable to the second-order spectrum of Si for wave-number shifts less than 125 cm^{-1}.

Away from the exciting laser frequency the background consists mainly of fluorescence from impurities in the diamond anvils. Although one can draw some general conclusions concerning the fluorescence spectra of diamonds,[17] the best way to determine the suitability of a pair of anvils is to measure their fluorescence. We have found that there is much variation among different diamonds, and that type-I diamonds may or may not be better than type-II diamonds. However, usually the over-all fluorescence level in the region of interest is lower for red excitation (e.g., 6471-Å Kr^+ or 6328-Å He-Ne) than for green or blue excitation (e.g., 5145- and 4880-Å Ar^+). In the present experiments, type-I diamonds were used, and, except where noted below, the exciting laser lines were 6471-Å Kr^+ for Si and 6328-Å He-Ne for GaP. If a chip of ruby has been placed in the cell in order to measure the pressure, one must take care that the Raman and ruby fluorescence spectra do not interfere. Since the ruby R lines are quite intense, and are accompanied by several phonon sidebands, it may be difficult to separate the two spectra if the laser frequency has been chosen too close to the R lines. On the other hand, the level of fluorescence from the diamonds may become intolerable if the excitation frequency is chosen too far into the green. Because of this problem the rather weak second-order Raman spectrum of Si was measured with no ruby in the diamond cell. The pressure was determined by simultaneously recording the shift of the first order peak (~ 35 times stronger),[28] which had been calibrated using the ruby R-line shift in a separate experiment. Without employing this procedure the optical overtone spectrum of Si would have been seriously obscured by ruby fluorescence.

The Waspaloy diamond-anvil cell weighs about 1.5 kg, and it is desirable to hold it in a strong stable mount. One must position the sample or ruby chip within the focused laser beam which can be reduced without difficulty to ~ 20 μm in diameter inside the cell. Some realignment is necessary each time the pressure is changed, especially at high pressure, where a considerable amount of torque is required to turn the pressure screw. Cell alignment is greatly simplified if there is some means for viewing the gasket hole and sample while making the necessary adjustments. This is conveniently accomplished by illuminating the gasket hole from behind with a bright lamp and observing the cell contents with a removable magnifying periscope device (such as the Spex model No. 1450) positioned at the monochromator entrance slits (refer to Fig. 2). It is also useful to observe the gasket hole while changing the pressure in order to ascertain the onset of gasket failure.

Our apparatus employed two lens fore optics with a collection lens of $f/1$ (nominally) and a magnification of $X8$ at the entrance slits. A Spex 1401 double monochromator with a photon-counting detection system was used. The spectra were recorded in an analog fashion using a ratemeter (for GaP) or were stored in the 400 channels of a multichannel analyzer and then plotted at the completion of each run (for Si). In the latter case each channel corresponded to a given frequency interval, typically 1 cm^{-1} for second-order and 0.15 cm^{-1} for first-order spectra. The monochromator spectral slit width was 3 cm^{-1}. Scan times were approximately 6 h for a 350-cm^{-1} interval. The He-Ne laser produced about 40-mW of useful power (after filtering) at 6328 Å, and the krypton-argon laser tube yielded about 100 mW at 6471 Å (also after filtering).

The GaP and Si samples were undoped (for GaP $n \sim 10^{15}$ cm^{-3}; for Si $p \sim 10^{14}$ cm^{-3}) unoriented single crystals. They were prepared by chipping larger single crystals under a microscope with a razor knife. Samples were approximately 100 μm in diameter, and 30 μm thick for Si, 30–60 μm thick for GaP. Although the appearance of cleavage planes gives some indication of orientation, definite knowledge of crystal orientation would require Laue x-ray-diffraction patterns from a 100-μm sample within the diamond cell, a difficult task at best, which we did not attempt. Therefore, with the orientation of the samples unknown, we did not investigate the polarized Raman spectra at high pressure.

BACKGROUND CONSIDERATIONS

For both Si and GaP the phonon dispersion at 1 atm is well known, having been studied by inelastic neutron scattering by Dolling (Si),[29] and Yarnell *et al.* (GaP).[30] By fitting multiparameter shell models to the neutron data, phonon frequencies away from high-symmetry directions have been determined reasonably well. There have been calculations of the density of phonon states for these and similar materials by Dolling and Cowley[31] and Kunc *et al.*,[32] but the most reliable picture of the density of states for Si comes from the neutron-scattering measurements of Nilson and Nelin for

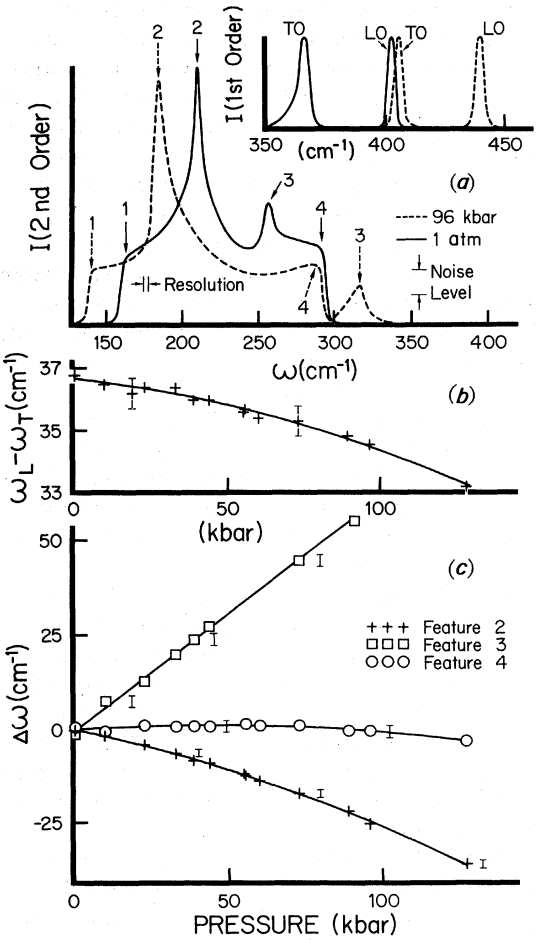

FIG. 3. (a) Measured first- and second-order room-temperature Raman spectra of GaP at 1 atm and 96 kbar. Intensity scales are arbitrary. (b) Energy splitting of the one-phonon peaks as a function of pressure. (c) Frequency shift of features 2–4 (see Table I and text for assignments) as a function of pressure. Features 1 (omitted for clarity) and 2 have a similar pressure dependence. Note the large positive shift for the difference mode, feature 3. For clarity, error flags are displaced.

Ge.[33,34] Due to the near homology of Si and Ge, the form of their respective densities of states is expected to be similar.[35] For GaP the density of transverse acoustical modes takes the same form as for Si and Ge, but there are differences in the optical-phonon region due to the nondegeneracy of TO and LO modes at Γ.

The effect of pressure on the phonon dispersion is described in terms of mode-Grüneisen parameters γ_i defined by

$$\gamma_i = -\frac{\partial \ln \omega_i}{\partial \ln V} = \frac{1}{\chi_T \omega_i}\left(\frac{\partial \omega_i}{\partial p}\right) , \tag{1}$$

where ω_i is a phonon frequency, χ_T is the isothermal compressibility, V is the crystal volume, and P is the pressure. The average Grüneisen constant γ is given by[36]

$$\gamma = \sum_i \gamma_i C_i \Big/ \sum_i C_i = \frac{V\beta}{\chi_T C_V} , \tag{2}$$

where C_i is the heat capacity of a single harmonic oscillator of frequency ω_i, C_V is the crystal heat capacity at constant volume, and β is the volume thermal-expansion coefficient. Therefore, if the mode-Grüneisen parameters are known for all branches throughout the zone, the thermal expansion can be calculated using

$$\beta(T) = \frac{1}{V}\int K_B \left(\frac{\hbar\omega}{K_B T}\right)^2 \frac{e^{\hbar\omega/K_B T}}{[e^{\hbar\omega/K_B T}-1]^2} \times \left(\frac{\partial\omega/\omega}{\partial P}\right)\rho(\omega)\, d\omega , \tag{3}$$

where $\rho(\omega)$ is the density of phonon states, T is the temperature, and K_B is the Boltzman constant.

The first- and second-order Raman spectra of Si[28,37,38] and GaP[12,38,39] have also been thoroughly investigated at atmospheric pressure, and because of the reliable neutron results, these spectra are well understood. Si (diamond cubic) has one first-order Raman peak, denoted O(Γ), occurring at 519.5 ± 1 cm^{-1}, and GaP (zinc-blende structure) has two first-order peaks, the LO(Γ) at 402.5 ± 1 cm^{-1}, and the TO(Γ) at 365.5 ± 1 cm^{-1} (ambient conditions). The strongest contributions to the two-phonon scattering come from zone-boundary modes, which are most numerous. For the cubic systems under consideration the second-order spectra consist of three symmetry components labeled by the irreducible representations Γ_1, Γ_{12}, and $\Gamma_{25'}$ for Si, and Γ_{15} for GaP.[40,41] It has been determined for both materials that the two-phonon spectra are dominated by the Γ_1 component which is chiefly comprised of scattering from overtone modes. The $\Gamma_{25'}$ (Γ_{15}) component is weaker containing contributions from many two-phonon combination modes, and the Γ_{12} component is very weak, almost negligible.[12,28,37–39] Furthermore, for both Si and GaP the form of the two-phonon Γ_1 component closely resembles the shape of the density of overtone states, i.e., the one-phonon density with a doubled-frequency scale. This is especially true for scattering by acoustical overtone modes for which the Raman spectra of GaP,[12] Si,[28,37] and Ge,[42] are very similar in form to each other and to the measured (neutron-scattering) density of states for Ge.[34] For scattering by optical overtone modes this result remains valid. However, for Si it is necessary to include some broadening of the Ge phonon density (measured at 80 K),[34] and for GaP, due to the nondegeneracy of TO(Γ) and LO(Γ) phonons, one must resort to comparison with the various calculations available for III-V

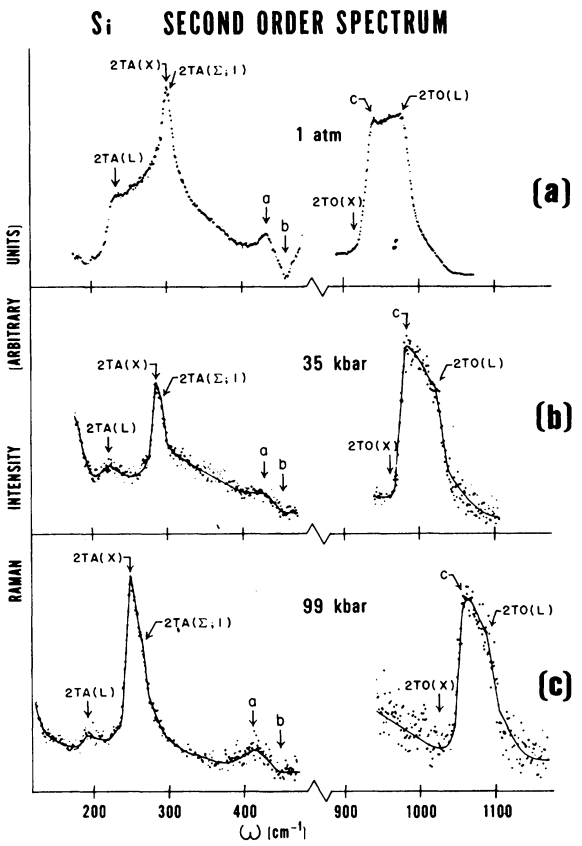

FIG. 4. Measured room-temperature two-phonon Raman spectra of Si at (a) 1 atm; (b) 35 kbar; and (c) 99 kbar. Only the regions of strong acoustical and optical overtone scattering are shown. Solid lines drawn (by sight) through the data in (b) and (c) show the smoothed spectra. Critical-point assignments based on neutron-scattering results are also indicated (see Table I). Spectral feature labels *a*, *b*, and *c* each designate several closely spaced singularities. Intensity units are arbitrary and different at each pressure. The 1-atm spectra were excited with 5145-Å light; otherwise 6471-Å excitation was used. Accordingly, the resonance effect discovered by Klein *et al.*[52] is observed at *c*. No appreciable pressure-induced resonance effects were found.

materials.[31,32] Since the over-all shape of the Raman spectra do not appear to change drastically upon application of hydrostatic pressure, one may assume that this result also holds at higher pressure. The resemblance of the second-order Raman spectra (dominated by their Γ_1 components) to the density of phonon states is an important result which simplifies the analysis of the effect of hydrostatic pressure on the phonon dispersion.

With the help of the neutron-scattering results the critical points associated with the major features in the second-order spectra of Si and GaP have been determined [see the assignments in Figs. 3(a) and 4, and Table I]. In the discussion of pressure effects which is to come, it should be kept in mind that the frequency shift of a given Raman structure reveals the pressure behavior of a number of phonons in some neighborhood of the critical point associated with this structure. For example, the major peak in the acoustical-overtone spectra of both these materials is bounded by the critical points 2TA(X) and 2TA(Σ; 1) [refer to Figs. 3(a) and 4], where the critical point along Σ occurs near K. However, the peak itself is due to scattering from a great many near-zone-boundary phonons lying in the region between these two critical points where the phonon dispersion is very flat. Consequently, the shift of this peak describes (with little variation) the pressure behavior of all the phonons in this region. Furthermore, a simple interpolation of pressure shifts between critical points based on frequency should not introduce too much error. This was found to be the case in our calculation of the thermal expansion of Si.

The well-known first-order semiconductor-to-metal transition occurring in Sn at atmospheric pressure and 286 K is accompanied by a change in structure from the diamond cubic (grey, α-Sn) to the body-centered tetragonal (white, β-Sn) form with a volume decrease of 20.9%.[44,45] This transition is often thought of as a prototype for the tetrahedral semiconductors. Pressure-induced transitions to phases of high conductivity in several Group-IV, III-V, and II-VI materials were first studied by Drickamer *et al.*[6] In Si a sudden drop of over five orders of magnitude in the resistance was found in the 120–150-kbar range, and in GaP a similar transition recently has been observed.[46] Van Vechten has presented a theory of this type of transformation in which the semiconducting and metallic phases are treated according to the Penn model and free-electron-gas approximation, respectively.[45] His calculated transition pressures (300 K) are in fair agreement with the available experimental data. The high-pressure x-ray-diffraction investigations of Jamieson and others[47] have demonstrated that Si initially transforms to the metallic β-Sn form (Si II), but after maintaining high pressure for several days a new phase called Si III, having a bcc structure with 8 atoms/(unit cell), develops. It also was found that Si III can be retained metastably at atmospheric pressure. Similar x-ray-diffraction studies of GaP are presently being performed in our laboratory.

HIGH-PRESSURE RESULTS

The room-temperature first-order Raman peaks recorded for Si at 1 atm and 35 and 99 kbar are displayed in Fig. 5(a). The peak shifts to higher energy with increasing pressure, and its frequency is plotted as a function of pressure in Fig. 5(b). The observed width is a combination of instrumen-

TABLE I. Two-phonon overtone assignments for Si and GaP. These assignments are based on the inelastic-neutron-scattering results of Refs. 29, 30, and 33–35. The notation is fully explained in the text. The quoted atmospheric-pressure room-temperature two-phonon frequencies and associated maximum uncertainties are from the present Raman work. For GaP the difference mode, feature 3 (Fig. 3), is excluded from this table.

		Si (Fig. 4)		GaP (Fig. 3)	
Critical-point assignment	Type of singularity	Figure designation	Frequency (1 atm) (cm^{-1})	Figure designation	Frequency (1 atm) (cm^{-1})
2TA(L; 1, 2)	P_1	2TA(L)	231 ± 3	1	164 ± 1
2TA (X; 1, 2)	P_1	2TA(X)	302 ± 1	2	209.4 ± 0.5
2TA (Σ; 1)	P_2	2TA (Σ; 1)	304 ± 2	2	209.4 ± 0.5
2TA (W; 1, 2)	P_3, P_1	a	433 ± 3	4	288 ± 2
2A (Q; 2)	P_2	a	433 ± 3		
2A (Σ; 2)	P_2	b	457 ± 4	4	288 ± 2
2A ($L-K$; 2)	P_3	b	457 ± 4		
2TO (X; 5, 6)	P_0	2TO(X)	921 ± 4		
2O (Q; 5)	P_1	c	942 ± 5		
2O (S_I; 5)	P_2	c	942 ± 5		
2TO (W; 5, 6)	P_3, P_1	c	942 ± 5		
2TO (L; 5, 6)	P_2	2TO(L)	979 ± 3		

tal resolution and intrinsic broadening (~ 3.5 cm^{-1}).[28] The peak is symmetric and there is no appreciable change in its line shape with applied pressure, as is the case for the TO(Γ) mode in GaP (see Fig. 6). Due to the strength of the one-phonon peak and its large pressure shift, we were able to accurately calibrate its position as a function of pressure using the ruby R_1-line fluorescence. This calibration is represented by the solid curve in Fig. 5(b) which is the best quadratic least-squares fit to the data (see figure caption). In subsequent measurements of second-order Si spectra this calibration was used to determine the pressure.

The first-order spectra of GaP measured at 1 atm and 96 kbar (room temperature) are shown in Fig. 3(a). Both the TO(Γ) and LO(Γ) peaks shift to higher energy with increasing pressure (as for Si), while their splitting, $\omega_L - \omega_T$, decreases. $\omega_L - \omega_T$ is plotted in Fig. 3(b), where we see that, although the decrease is small, it is certainly beyond experimental uncertainty. This result contradicts previous low-pressure ($\lesssim$10 kbar) measurements for GaP which determined a marginal increase in $\omega_L - \omega_T$, but agrees with measurements on ZnS, ZnSe, and ZnTe for which a larger effect was found.[7,12]

The effect of pressure on the line shape of the TO(Γ) peak in GaP is displayed in Fig. 6(a). At atmospheric pressure this peak is asymmetric toward the low-energy side, but as the pressure is increased the asymmetry lessens. Plotted as a function of pressure in Fig. 6(b) is the asymmetric portion of the peak width, $\Delta_2 - \Delta_1$; at ~ 80 kbar the peak has become symmetric. The pressure data are consistent with an explanation proposed by Barker[48] that the TO(Γ) asymmetry is due to the anharmonic interaction of the TO(Γ) phonon with the nearly degenerate (at 1 atm) combination mode TA(X) + LA(X). The negative pressure coefficient $d\omega/dp$ of the TA(X) mode (see discussion below) will tend to reduce the pressure coefficient of the combination, giving it a small positive or even negative value. Thus, the near degeneracy with TO(Γ), which has a large positive pressure coefficient, should not be present at high pressure.

Figures 3(a) and 4 exhibit the effect of pressure on the measured second order Raman spectra of GaP and Si, respectively. For GaP only the second-order spectrum in the region of acoustical overtone scattering is shown, while for Si the Raman spectra in both the acoustical and optical-overtone regions are displayed. The optical-overtone spectrum of GaP was seriously obscured by a strong luminescence background and was not investigated at high pressure. For both materials the scattering, which lies in frequency between the first-order peaks and optical-overtone regions and consists of combination bands and overtones of longitudinal modes,[12,28] was not studied due to its relatively weak intensity. The spectra shown in Figs. 3(a) and 4 consist of arbitrary mixtures of the three possible symmetry components, but as discussed above we can be sure that the Γ_1 component, reflecting the shape of the phonon density of states, is dominant. Note the similarity between the acoustical-overtone spectra for both materials.

Critical-point assignments based on the neutron

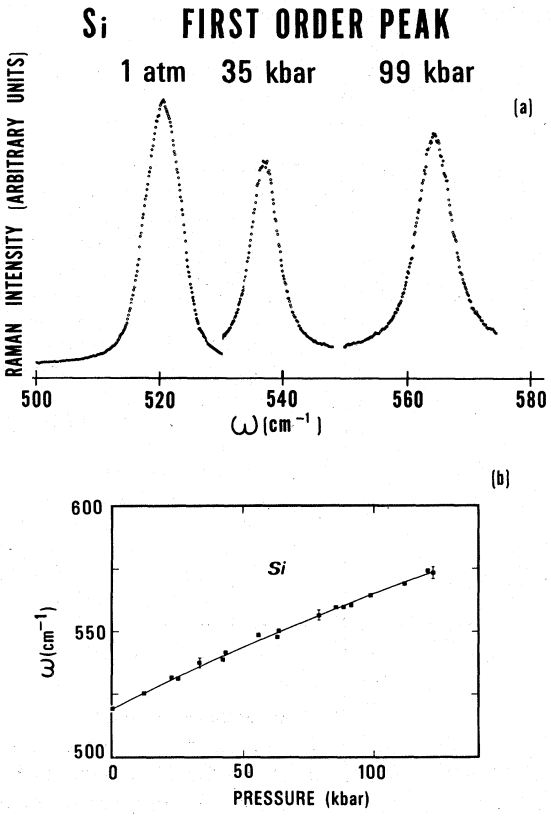

FIG. 5. (a) First-order Raman spectrum of Si measured at room temperature for pressures of 1 atm and 35 and 99 kbar. The intensity scale is different for each peak. (b) Frequency of the first-order peak plotted as a function of pressure showing experimental results (squares), and best quadratic least-squares fit (solid line). The equation of this fit is

$$\omega = 519.5 \pm 0.8\ \text{cm}^{-1} + (0.52 \pm 0.03\ \text{cm}^{-1}\ \text{kbar}^{-1})P + (-0.0007 \pm 0.0002\ \text{cm}^{-1}\ \text{kbar}^{-2})P^2 .$$

Maximum uncertainties are indicated by the error flags.

data[29,30,34] designate the major features in the second-order spectra in Figs. 3(a) and 4. A key to these assignments appears in Table I. In this table we present the critical-point assignments, the associated singularity types,[49] and for each material the assignment designation in the figures, and the corresponding atmospheric-pressure room-temperature second-order Raman frequencies. If the vibration associated with a particular critical point is not purely transverse or longitudinal, only its acoustical (A) or optical (O) character is stipulated. The number(s) within parentheses following each critical-point designation labels the phonon branch(es) (in order of increasing energy) containing that point; if two branches are degenerate, both numbers occur. For example, 2TA(L; 1, 2) refers to the overtone of phonons from the critical point at L in the first and second transverse acoustical branches. Using the notation of Ref. 50, the Q point lies on the line $L-W$, $L-K$ designates a point on the line L-K and S_I denotes a critical point in the $q_z = 0$ plane not on a symmetry line. At the W point branches 1 and 5 have P_3-type, and 2 and 6 P_1-type singularities. There were several nearly degenerate critical points, usually including points of low symmetry, which we were unable to resolve in our high-pressure measurements; these points were lumped under common labels (a, b, c, etc.). It was assumed, in such cases, that the pressure shifts of each of the closely spaced points were approximately the same and were given by the shift of some average position (e.g., the shoulder a in Fig. 4). Because the neutron data for GaP are not so complete as for Si (and Ge), the identity of the shoulder labeled 4 in Fig. 3(a) is not so well established. Contributions from around the W point in branches 1 and 2 and from the second branch along Σ are indicated. The small peak labeled 3 in Fig. 3(a) has been identified with one of the difference modes TO(X) − TA(X) or TO(L) − TA(L) by its characteristic temperature dependence[39,51] and large positive pressure coefficient (see discussion below). A detailed account of these assignments can be found in Refs. 12, 28, and 37–39.

Upon application of hydrostatic pressure, the two-phonon Raman spectra [see Figs. 3(a) and 4]

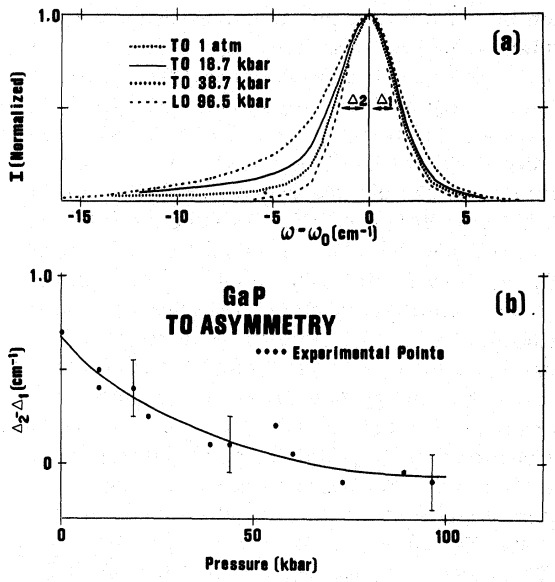

FIG. 6. (a) Comparison of the asymmetric first-order TO(Γ) peak in GaP at three different pressures and the symmetric LO(Γ) peak at 96.5 kbar. The TO(Γ) asymmetry decreases with pressure. The peak intensities are all normalized to unity. (b) Plot of the asymmetric portion of the TO(Γ) peak width $\Delta_2 - \Delta_1$ as a function of pressure. At ~80 kbar the TO(Γ) peak is symmetric.

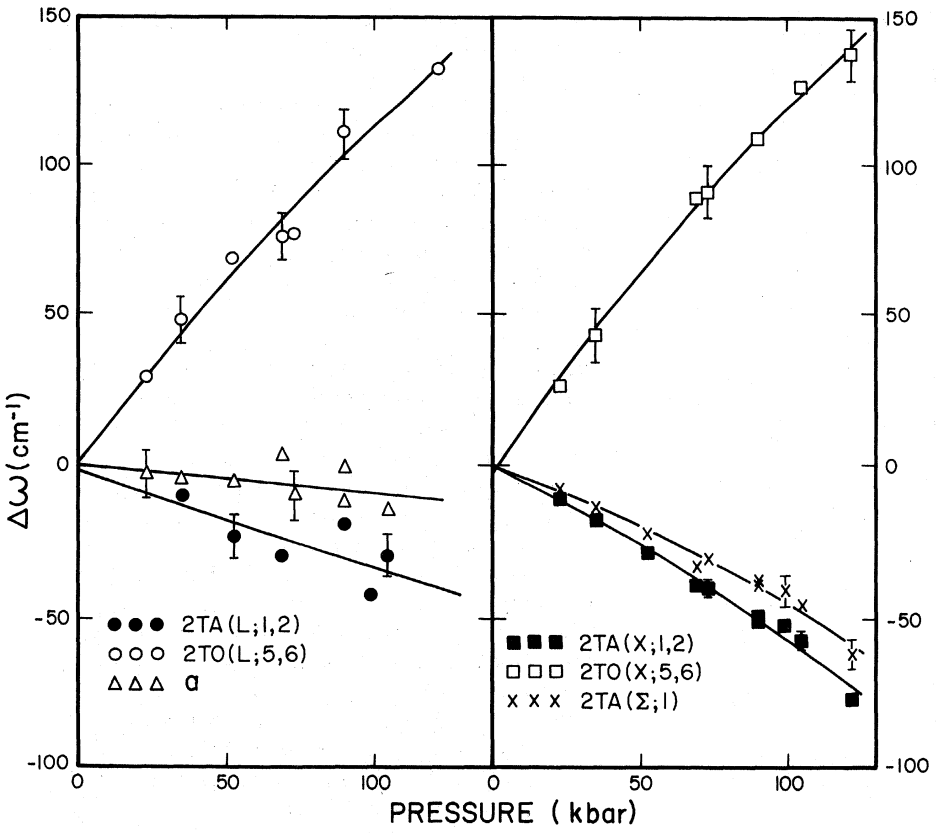

FIG. 7. Frequency shift as a function of pressure observed for several critical points in the two-phonon Raman spectrum of Si (see Fig. 4). Estimates of maximum uncertainty are indicated by the error flags accompanying experimental points. Solid curves are best least-squares fits to the data (see Table II). Features *b* and *c* (Fig. 4) are omitted for clarity; refer to Table II for corresponding best-fit pressure coefficients. Note contrast of positive and negative shifts for zone-boundary TO and TA modes.

maintain their general shape but shift by different amounts and in different directions depending on the particular phonons under consideration. For both Si and GaP the data shows that TA modes in the neighborhood of the L point, and extending from X to a critical point along Σ (near K) in branch 1, have negative pressure coefficients. In contrast, the entire optical-overtone spectrum of Si in Fig. 4, including the TO overtone modes in the vicinity of X and L, and those denoted by c (refer to Table I), shifts to higher energy with applied pressure. Similarly for GaP the measurements ($\lesssim$10 kbar) of Ref. 12 indicate positive pressure coefficients for the major TO and LO overtone structures in the second-order spectrum of this material. The features labeled a and b in Fig. 4, and labeled 4 in Fig. 3(a) (refer to Table I) show only a weak pressure dependence.

In Figs. 3(c) and 7 the frequency shifts of the various critical points observed in the two-phonon Raman spectra of GaP and Si are plotted as a function of pressure. Estimates of maximum experimental uncertainty are indicated by the error flags accompanying several of the data points. The solid curves are best least-squares fits to the data; in some cases, quadratic terms were appreciable, and in others linear fits sufficed. The parameters obtained from these fits and their maximum estimated uncertainties are listed in columns 1–4 of Table II. Linear-pressure coefficients are presented in terms of the mode-Grüneisen parameters γ_i defined in Eq. (2), and quadratic pressure coefficients are given by half the second derivative of the phonon frequency with respect to pressure.

The contrast between the positive and negative pressure shifts of TO and TA phonons at X and at L is clear in Fig. 7 for Si. The shift of the critical point 2TA(Σ;1) is also plotted there. At atmospheric pressure this critical point is separated from 2TA(X) by only ~ 2 cm^{-1}, and it is often difficult to resolve the two. However, the frequency splitting of these singularities increases with applied pressure (see Fig. 7), and at high pressure they can be resolved without difficulty. This is illustrated in Fig. 8, where the sharp peak in the acoustical-overtone spectrum of Si measured at 70 kbar has been displayed using an expanded frequency scale. The two critical points 2TA(X) and 2TA(Σ;1) are clearly visible at this pressure and their splitting has increased to 9 cm^{-1}. The topological nature of these singularities, P_1 for 2TA(X) and P_2 for 2TA(Σ;1), is also evident. This example demonstrates the use of very high pressure to identify nearly degenerate critical points. For

TABLE II. One-phonon quadratic-pressure coefficients $[\frac{1}{2}(d^2\omega/dp^2)]$ and mode Grüneisen parameters γ_i measured for GaP and Si in this work. Values obtained from best least-squares fits to measured pressure shifts of critical-point spectral features (see Figs. 3–5 and 7). Associated maximum uncertainties are shown. The compressibilities of Si and GaP, needed to compute γ_i, were taken from Refs. 2 and 43, respectively. Also listed for comparison (see discussion in text) are other experimental and theoretically predicted values of γ_i for Si, GaP, Ge, and ZnTe by several authors. Note the discrepancy between theory and experiment for the γ_i of zone boundary TA modes in Si.

	Si[a]	GaP[b]	Si	GaP	Ge	ZnTe
	$\frac{1}{2}\frac{d^2\omega}{dP^2}$	$\frac{1}{2}\frac{d^2\omega}{dP^2}$				
	$\left(10^{-4}\frac{\text{cm}^{-1}}{\text{kbar}^2}\right)$	$\left(10^{-4}\frac{\text{cm}^{-1}}{\text{kbar}^2}\right)$	γ_i	γ_i	γ_i	γ_i
TO(Γ)	-7 ± 2	-3.6 ± 0.7	0.98 ± 0.06[a] 1.02 ± 0.02[c] 1.06[h]	1.09 ± 0.03[b] 1.19 ± 0.04[e] 1.07 ± 0.1[d]	1.12 ± 0.02[c] 1.23[f] 1.13[h]	1.6 ± 0.1[d] 1.5[g]
LO(Γ)	-7 ± 2	-4.2 ± 0.8	0.98 ± 0.06[a] 1.02 ± 0.02[c] 1.06[h]	0.95 ± 0.02[b] 1.16 ± 0.04[e] 1.1 ± 0.1[d]	1.12 ± 0.02[c] 1.23[f] 1.13[h]	1.0 ± 0.1[d] 0.75[g]
TA(L; 1, 2)	...	-4.0 ± 0.5	-1.3 ± 0.3[a] -0.25[h]	-0.81 ± 0.07[b]	-0.4 ± 0.3[i] -0.29[f] -0.1[h] -0.2[k]	-0.15[g] -1.1[j]
TA(X; 1, 2)	-7 ± 3	-4.4 ± 0.3	-1.4 ± 0.3[a] -1.4 ± 0.2[l] -0.6[h]	-0.72 ± 0.03[b] -0.60 ± 0.07[e]	-0.35[f] -0.23[h] -0.38[k]	-0.2[g]
TA(Σ; 1)	-6 ± 3	-4.4 ± 0.3	-1.0 ± 0.3[a] -0.17[h]	-0.72 ± 0.03[b] -0.60 ± 0.07[e]	-0.05[h] -0.3[k]	-0.2[g]
TA(W; 1, 2) A(Q; 2)	...	...	-0.2 ± 0.1[a]	...	...	...
$A(\Sigma; 2)$ $A(L-K; 2)$	...	-3.1 ± 0.5	-0.3 ± 0.1[a] -0.3[h]	0.15 ± 0.03[b]	-0.1[h] -0.3[k]	-0.1[g]
TO(X; 5, 6)	-11 ± 4	-4.4 ± 0.6[m]	1.5 ± 0.1[a] 1.3[h]	1.31 ± 0.05[b,m]	1.6[f] 1.4[h]	1.6[g]
O(Q; 5) O(S_I; 5) TO(W; 5, 6)	-10 ± 5	...	1.5 ± 0.1[a]	...	...	...
TO(L; 5,6)	-10 ± 7	-4 ± 1[m]	1.3 ± 0.2[a] 1.18[h]	1.40 ± 0.08[b,m] 1.50 ± 0.05[e]	1.42[f] 1.27[h] 0.9 ± 0.1[i]	1.73[g]

[a]Present work.
[b]Reference 19 measured.
[c]Reference 10 measured.
[d]Reference 7 measured.
[e]Reference 12 measured.
[f]Reference 31 calculated.
[g]Reference 62 calculated.
[h]Reference 57 calculated.
[i]Reference 60 measured.
[j]Reference 8 measured.
[k]Reference 61 calculated.
[l]Reference 63 measured.
[m]Deduced from shift of TO-TA difference mode.

GaP these two points remained unresolved at high pressure.

Also plotted in Fig. 7 is the pressure shift of the feature labeled *a* in the two-phonon spectrum of Si (see Fig. 4). Its pressure behavior is to be compared with that of the shoulder labeled 4 in the GaP spectrum [refer to Figs. 3(a) and (c)]. Both structures shift only slightly with pressure.

The small peak denoted 3 in the GaP spectrum [Fig. 3(a)] shifts strongly to higher energy with applied pressure; its pressure shift is plotted in Fig. 3(c). This behavior, which differs from that of the rest of the acoustical-overtone spectrum, indicates a zone boundary TO-TA–type difference mode.[53] Furthermore, the intensity of this peak displays a temperature dependence characteristic

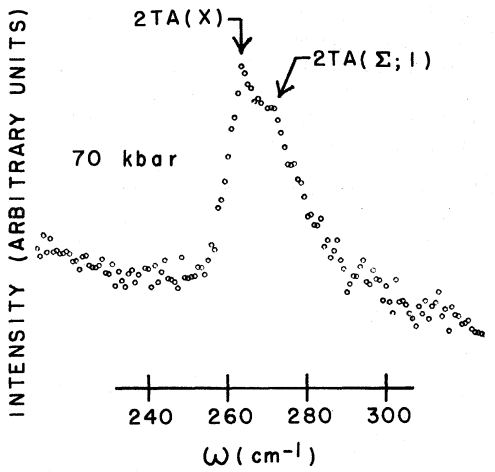

FIG. 8. Strong peak in the acoustical overtone spectrum of Si (Fig. 4) measured at 70 kbar and plotted on an expanded frequency scale. At this pressure 2TA(X) and 2TA(Σ; 1) are separated by ~9 cm^{-1} and clearly resolved.

of a difference mode.[39,51] The only energetically possible assignments are TO(X) – TA(X) or TO(L) – TA(L).[39] However, in either case the derived γ_{TO} (using the measured γ_{TA}) agree favorably with the results of Ref. 12, assuming γ_{TO} to be about the same at X and L (see Table II). Thus, one cannot rule out either possibility. The counterpart of this difference mode does not appear in Si.

For Si it was found that at ~125 kbar the Raman intensity decreased sharply. This is illustrated in Fig. 9 where the first-order peak intensity is plotted on a semilog scale as a function of pressure. We interpret this result as signaling a phase transition to a modification of Si with different Raman structure. Unfortunately, the Raman spectrum of the new phase was too weak to be detected indicating a highly opaque form.[54] To further investigate this transition we employed a Research Devices Inc. model D infrared microscope in order to visually observe a Si sample at high pressure. In an independent experiment using this device a piece of Si viewed at low pressure within the diamond-cell appeared transparent. At 125 ± 5 kbar the sample became completely opaque, and this transformation was not a gradual one (in time) but rather appeared in a portion of the Si and spread throughout the sample within ~5 min (at constant pressure).[55] The pressure and rapidity of this transformation, in both the Raman and visual experiments, indicate that it was the semiconductor-to-metal (β-Sn structure) transition observed in high pressure x-ray-diffraction studies of Si.[47] We also found that samples held at high pressure for several days did not reveal the diamond cubic Raman spectrum upon lowering of pressure. This behavior is consistent with the formation of metastable Si III. However, our attempts to measure the Raman spectrum of Si III[56] for material retrieved from the cell were unsuccessful, probably due to the poor optical quality and small quantity of material removed.

Consistent with the first-order nature of the $\alpha - \beta$ transformation (~20% volume change), none of the observed modes with negative pressure coefficients attained zero frequency at the transition pressure. For example, the frequency of TA(L) at 125 kbar is 95 cm^{-1}.

DISCUSSION

Our analysis of the effect of pressure on the second-order Raman spectra of Si and GaP has focused on certain critical points such as L, X, Σ, etc., whose pressure shifts are easily measured because they are associated with pronounced features in the spectra. However, because of the density-of-states character of the two-phonon spectra, the data actually reveal the pressure dependence of the phonon dispersion over a large portion of the Brillouin zone, especially in the region near the zone boundary. Consequently, it is not hard to perceive certain general trends which we now discuss.

In both materials zone-boundary phonons belonging to the lowest acoustical branch shift to lower energy with increasing pressure. This result applies to the rather flat portion of the first branch extending from (and in the vicinity of) K (U) to X and from K (U) to L (see Refs. 29, 30, 33, and 50). Furthermore, for each material the similar values of the mode-Grüneisen parameters at L, X, and (Σ;1) (~ –1.25 for Si and ~ –0.75 for GaP,

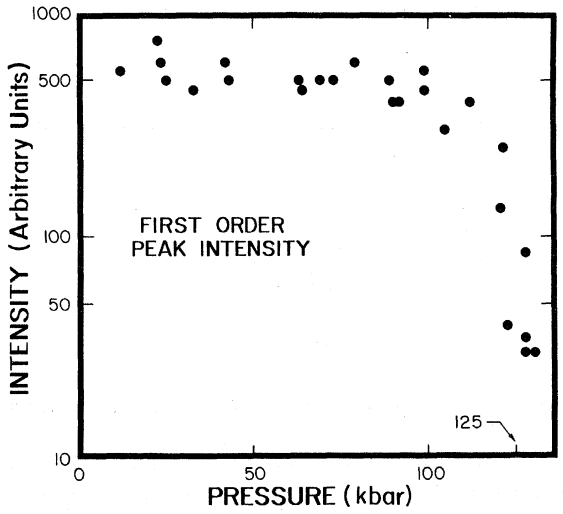

FIG. 9. Semilog plot of first-order peak intensity as a function of pressure for Si. Intensity extrapolates to zero at ~125 kbar indicating transformation to a different phase.

see Table II) indicate a fairly uniform shift. Thus, this portion of the lowest phonon branch retains its flat character at high pressure. For the second acoustical branch in the neighborhood of the zone edge (for directions where branches 1 and 2 are not degenerate), our results indicate only a slight dependence on pressure.

The optical branches move to higher energy with increasing pressure. This is true of both zone-center and zone-boundary modes. The uniform shift of the optical-overtone spectrum of Si in Fig. 4, and the similar values of γ_i in Table II for TO(X), TO(L), TO(W; 5, 6), etc. (all ~1.4 for Si and all ~1.35 for GaP), show that zone edge phonons from the upper two branches behave similarly under pressure. However, because the mode-Grüneisen parameters for $\vec{q}=0$ phonons in these materials are only ~1.0, branches 5 and 6 will tend to flatten with increasing pressure.

The pressure dependence of zone-boundary longitudinal (optical and acoustical) phonons has not been investigated in our experiments. From the predictions of various calculations we expect these modes to have positive Grüneisen parameters of intermediate value ranging approximately from 0.5 to 1.3.[31,57]

An aspect of the general pressure behavior outlined above that is expected to apply to other tetrahedral semiconductors is the negative-pressure coefficients of zone-boundary TA modes. This accounts for the negative thermal-expansion coefficients usually found at low temperature in these materials.[3,58] As pointed out by Blackman,[36] the thermal-expansion coefficient may become negative if low-frequency modes, which dominate the sum in Eq. (2) at low temperature, possess negative γ_i. Furthermore, the largest contribution to the thermal expansion will come from zone-boundary phonons because of the density-of-states factor in Eq. (3). To illustrate these points we have performed a calculation of the volume thermal expansion of Si, $\beta(T)$, as a function of temperature based solely on our Raman data. Equation (3) was evaluated numerically using the measured phonon frequency shifts, $\partial\omega/\partial p$. The pressure shift of noncritical-point phonons was simply determined by interpolating linearly with frequency between critical points. For the phonon density of states we used the atmospheric-pressure overtone Raman spectrum shown in Fig. 4(a). The frequency scale was divided by 2, and the optical-overtone intensity was multiplied by a constant in order that the relative weight of acoustical and optical modes should approximately correspond to that of the Ge density of states measured in Ref. 34.

The result of this calculation is displayed in Fig. 10 by the solid curve. Although negative β coefficients are obtained at low temperature, and the general functional dependence on temperature has been reproduced, the calculated values are too small and deviate appreciably from the measured thermal-expansion coefficient of Si.[3] This is not surprising since we have neglected completely the contribution of zone-edge LA and LO modes. To include these phonons the density of states for Ge[34] in the appropriate region was adapted by changing the frequency scale to match that of Si. A single parameter, representing the average Grüneisen constant of all zone-boundary (or near zone boundary) LA and LO phonons, was varied so as to fit the calculation to the measured thermal expansion at 300 K.[59] The value $\gamma_{av}(\mathrm{LA;LO})\approx 0.9$ obtained for this parameter is consistent with theoretical predictions.[31,57] The dashed curve in Fig. 10 shows the result of this new calculation. The magnitude as well as the temperature dependence of $\beta(T)$ now compare favorably with direct measurements, and the calculated minimum occurs at the proper temperature, ~80 K. The deviation from experiment at the minimum is due to having neglected acoustic modes with frequency <100 cm^{-1}, which do not display an appreciable second-order Raman spectrum [see Fig. 4(a)]. At ~80 K the value of the Einstein specific-heat function [C_i in Eq. (2)] is such that low-frequency phonons of intermediate wavelength, for which the density of states is not negligible, can noticeably contribute to the thermal expansion. A small positive contribution is indicated for these

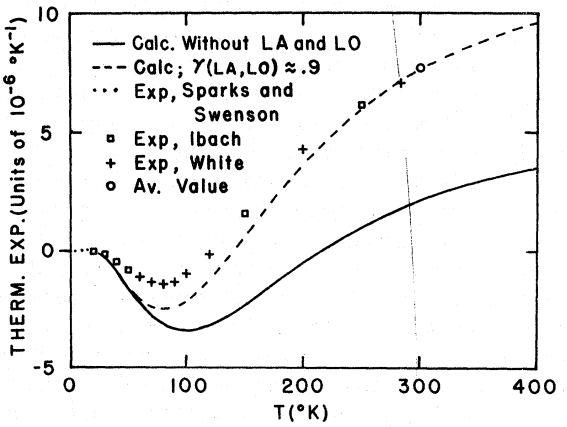

FIG. 10. Comparison of the volume thermal-expansion coefficient of Si (as a function of temperature) computed in this work and measured directly. Solid curve computed with no adjustable parameters using only the high-pressure Raman data and 1-atm two-phonon spectrum for the density of states (see text). Dashed curve, including contributions from zone-boundary LA and LO modes, is fit to the measured thermal expansion at 300 K using one adjustable parameter, $\gamma_{av}(\mathrm{LA;LO})\approx 0.9$ (see text). Experimental points were taken from the compilation by White (Ref. 3). The average value at 300 K was determined as indicated in Ref. 59.

modes by the ultrasonic measurements of McSkimin *et al.*[2] However, we do not pursue the subject further because our purpose is only to demonstrate that a calculation based on the second-order Raman data, which emphasizes the role of zone-boundary phonons, can reasonably account for the magnitude and temperature dependence of the thermal-expansion coefficient of Si, predicting negative low-temperature values.

Listed in Table II for comparison with the results of this work are the measured and theoretically predicted mode-Grüneisen parameters γ_i obtained for Si, GaP, Ge, and ZnTe by several different researchers (see table for references). Except for Payne's tunneling measurements in Ge,[60] the experimental results derive from low-pressure Raman-scattering measurements. The agreement among the experimental values in Table II is generally very good. Of the theoretical calculations, those of Jex,[57] Dolling and Cowley,[31] and Bienenstock[61] use one or more (up to three) adjustable parameters to obtain the best fit to the experimentally determined thermal expansion (or average Grüneisen constant) of the material under study. The fitting parameters are arrived at by assuming some model; for example, in the work of Jex the crystal potential is expanded in a double power series in terms of thermal strain parameters and atomic displacements, and two-body, central, first- and second-neighbor forces are included. The calculation of Vetelino *et al.*[62] for ZnTe involves a four-parameter rigid-ion model in which the phonon dispersion is completely determined by the TO(Γ) and LO(Γ) frequencies, and the elastic constants. The effect of pressure is included through the measured pressure dependence of these quantities. This model is not expected to work well for predominantly covalent materials.

Although these calculations reasonably depict the magnitude and general wave-vector dependence of the mode-Grüneisen parameters (arriving at negative values for zone boundary TA phonons), the predicted γ_i often differ substantially from the measured values of Table II. In particular, the calculations have largely underestimated the "lattice-softening" effect of pressure on TA modes at X, L, and $(\Sigma;1)$. Richter *et al.*[63] have pointed out that the theoretical treatment could be improved by including further neighbor forces. We further suggest that the large discrepancy for short-wavelength acoustical modes in branch 1 may be due to the neglect of noncentral forces in the models.

The characteristic low energy and flatness of the lowest acoustical branch away from the zone center in tetrahedral semiconductors has generally been difficult to understand theoretically. However, the phonon dispersion (1 atm) of Ge has recently been calculated with considerable success using a four-parameter dynamic bond-charge model.[64] In this model the flattening of the TA branch arises when the effective force between neighboring bond charges is much greater than the ion–bond-charge coupling. For TA modes of large $\vec{q}$ the ions then oscillate as Einstein oscillators in a nearly rigid "lattice" of bond charges with a frequency determined by the effective ion–bond-charge force. This force consists of short-range and Coulomb terms, which partially cancel, leading to a weak effective interaction. Consequently, the "softening" effect of pressure on zone-boundary TA modes implies a weakening of the effective ion–bond-charge coupling and the associated noncentral forces which help to stabilize the structure against short wavelength shear distortion.[65,66]

Since for α-Sn the metallic transformation occurs at 1 atm (286 K), it is interesting to compare the phonon dispersion of this material at 1 atm, with that of Si at its transition pressure, ~125 kbar. We do this by normalizing the phonon frequencies with the appropriate ion plasma frequency,[44]

$$\omega_p^2 = 4\pi(Ze)^2/mV_a\,, \tag{4}$$

where the valence is $Z=4$, V_a is the atomic volume, and the ion mass is m. Scaling the frequencies in this way eliminates differences due to mass and lattice constant so that any remaining differences must be due to varying effects of the valence electrons. Using the high-pressure Raman data for Si and the neutron results of Ref. 44 for α-Sn, we find that the scaled frequencies agree to within 1.5% for TA(X) (Si is higher) but differ by 8% for TO(X) (Si is higher) and 3.5% for TO(Γ) (Si is lower). Thus, at the transition pressure the zone-boundary configuration of the flat TA branch appears to be similar in both materials, indicating parallel behavior of the valence electrons for these modes.[64] A similar comparison (with Sn and with InSb)[44,67] was performed for GaP by extrapolating our high-pressure results to 216 kbar, the pressure predicted by Van Vechten[45] for the metallic transition in this material. No analogous correlation was found (scaled frequencies differed by ~25%), and it appears that for GaP, with atoms from two different rows of the Periodic Table, the situation is more complicated.

CONCLUDING REMARKS

By studying the Raman spectra of Si and GaP to ~135 kbar it has been possible to deduce the general effect of pressure on much of the phonon dispersion of these substances, especially in the Brillouin-zone boundary region. It is hoped that this work will stimulate further research of a similar nature. The mode-Grüneisen parameters so obtained will permit a more detailed test of theories of anharmonicity than comparison with the thermal-

expansion coefficient, and improved understanding of interatomic forces in predominantly covalent crystals should result. Detailed high-pressure Raman investigations of other tetrahedral semiconductors will allow further comparison of phonon frequencies at the metallic phase transition. This may reveal systematic trends related to the role of valence electrons in determining the frequencies of zone-boundary TA modes. Such trends are relevant to the bond-charge model, as the "softening" of these modes with pressure, which may be associated with instability to short-wavelength shear distortions, reflects weakening of the ion-bond charge interaction. Therefore, it would be interesting to compare the mode-Grüneisen parameters measured here for Si to those that would be predicted on the basis of the dynamic bond-charge model.

ACKNOWLEDGMENTS

The authors wish to thank B. Cohen of Research Devices, Inc. for demonstrating the use of the infrared microscope during our investigation of Si. Helpful discussions with A. H. Kahn, G. J. Rosasco, R. A. Forman, and B. Mozer are also appreciated.

---

*National Research Council–National Bureau of Standards Postdoctoral Research Associate, 1974–1975.

†Address after August 1, 1975: Dept. of Physics, Purdue Univ., West Lafayette, Ind. 47907.

[1]1 kbar = 10^9 dyn/cm^2.

[2]H. J. McSkimin and P. Andreatch, Jr., J. Appl. Phys. 35, 2161 (1964); J. B. Wachtman, Jr., in *Mechanical and Thermal Properties of Ceramics*, NBS Special Publication No. 303, edited by J. B. Wachtman, Jr. 1969, (unpublished), p. 139.

[3]R. K. Kirby (private communication). An excellent compilation of recent thermal-expansion data for Si and several other materials can be found in the following article: G. K. White, in *AIP Conference Proceedings No.* 17, *Thermal Expansions*-1973, edited by R. E. Taylor and G. L. Denman (American Institute of Physics, New York, 1974), p. 1.

[4]J. F. Scott, Rev. Mod. Phys. 46, 83 (1974).

[5]P. Peercy, Phys. Rev. Lett. 31, 379 (1973).

[6]S. Minomura and H. G. Drickamer, J. Phys. Chem. Solids 23, 451 (1962); G. A. Samara and H. G. Drickamer, J. Phys. Chem. Solids, 23, 457 (1962).

[7]S. S. Mitra, O. Brafman, W. B. Daniels, and R. K. Crawford, Phys. Rev. 186, 942 (1969).

[8]O. Brafman and S. S. Mitra, in *Proceedings of the 2nd International Conference on Light Scattering in Solids*, Paris, 1971, edited by M. Balkanski (Flammarion, Paris, 1971), p. 280.

[9]O. Brafman, S. S. Mitra, R. K. Crawford, W. B. Daniels, C. Postmus, and J. R. Ferraro, Solid State Commun. 7, 449 (1969).

[10]C. J. Buchenauer, F. Cerdeira, and M. Cardona, in *Proceedings of the 2nd International Conference on Light Scattering in Solids*, Paris, 1971, edited by M. Balkanski (Flammarion, Paris, 1971), p. 280.

[11]J. B. Renucci, M. A. Renucci, and M. Cardona, Solid State Commun. 9, 1651 (1971).

[12]B. A. Weinstein, J. B. Renucci, and M. Cardona, Solid State Commun. 12, 473 (1973).

[13]E. Anastassakis, A. Pinczuk, E. Burstein, F. H. Pollak, and M. Cardona, Solid State Commun. 8, 133 (1970); F. Cerdeira, C. J. Buchenauer, F. H. Pollak, and M. Cardona, Phys. Rev. B 5, 580 (1972).

[14]S. Venugopalan and A. K. Ramdas, Phys. Rev. B 8, 717 (1973).

[15]J. W. Brasch, A. J. Melveger, and E. R. Lippincott, Chem. Phys. Lett. 2, 99 (1968).

[16]C. Postmus, V. A. Maroni, J. R. Ferraro, and S. S. Mitra, Inorg. Nucl. Chem. Lett. 4, 269 (1968).

[17]D. M. Adams, S. J. Payne, and K. Martin, Appl. Spectrosc. 27, 377 (1973).

[18]Y. Yacoby, F. Cerdeira, M. Schmidt, and W. B. Holzapfel, Solid State Commun. 14, 1325 (1974); F. Cerdeira (private communication).

[19]B. A. Weinstein and G. J. Piermarini, Phys. Lett. 48A, 14 (1974).

[20]G. J. Piermarini and C. E. Weir, J. Res. Natl. Bur. Stand. (U. S.) A 66, 325 (1962).

[21]G. J. Piermarini and A. B. Braun, J. Chem. Phys. 58, 1974 (1973).

[22]S. Block and G. J. Piermarini, High Temp–High Pressures 5, 567 (1973).

[23]J. D. Barnett, S. Block, and G. J. Piermarini, Rev. Sci. Instrum. 44, 1 (1973).

[24]G. J. Piermarini, S. Block, and J. D. Barnett, J. Appl. Phys. 44, 5377 (1973).

[25]G. J. Piermarini, S. Block, J. D. Barnett, and R. A. Forman, J. Appl. Phys. 46, 2774 (1975).

[26]Since it is known that Si can withstand a uniaxial strain of ~20 kbar (Ref. 27) and GaP somewhat less, and we did not observe any breakup of our samples, we expect the stress gradiants inside the cell to be $\lesssim$ 20 kbar.

[27]F. H. Pollak and M. Cardona, Phys. Rev. 172, 816 (1968).

[28]P. A. Temple and C. E. Hathaway, Phys. Rev. B 7, 3685 (1973).

[29]G. Dolling, in *Symposium on Inelastic Scattering of Neutrons in Solids and Liquids* (IAEA, Vienna, 1963), Vol. II, p. 37.

[30]J. L. Yarnell, J. L. Warren, R. G. Wenzel, and P. J. Dean, in *The Fourth IAEA Symposium on Neutron Inelastic Scattering* (IAEA, Vienna, 1968), Vol. I, p. 301.

[31]G. Dolling and R. A. Cowley, Proc. Phys. Soc. Lond. 88, 463 (1966).

[32]K. Kunc, M. Balkanski, and M. A. Nusimovici, in *Proceedings of the Tenth International Conference on the Physics of Semiconductors*, Cambridge, Mass., 1970, (U. S. A. E. C., Oak Ridge, Tenn., 1970), p. 119.

[33]G. Nilsson and G. Nelin, Phys. Rev. B 3, 364 (1971).

[34]G. Nelin and G. Nilsson, Phys. Rev. B 5, 3151 (1972).

[35]G. Nilsson and G. Nelin, Phys. Rev. B 6, 3777 (1972).

[36]M. Blackman, Proc. Phys. Soc. Lond. B 70, 827 (1957).

[37]K. Uchinokura, T. Sekine, and E. Matsuara, Solid State Commun. 11, 47 (1972).

[38]B. A. Weinstein and M. Cardona, Solid State Commun. 10, 961 (1972).
[39]R. M. Hoff and J. C. Irwin, Can. J. Phys. 51, 63 (1973).
[40]R. Loudon, Adv. Phys. 13, 423 (1964).
[41]L. N. Ovander, Opt. Spectrosc. 9, 302 (1960).
[42]B. A. Weinstein and M. Cardona, Phys. Rev. B 7, 2545 (1973).
[43]R. Weil and W. O. Groves, J. Appl. Phys. 39, 4049 (1968).
[44]D. L. Price and J. M. Rowe, Solid State Commun. 7, 1433 (1969); D. L. Price and J. M. Rowe, Phys. Rev. B 3, 1268 (1971).
[45]J. A. Van Vechten, Phys. Rev. B 7, 1479 (1973).
[46]A. Onodera, N. Kawai, K. Ishizaki, and I. L. Spain, Solid State Commun. 14, 803 (1974).
[47]J. C. Jamieson, Science 139, 762 (1963); J. S. Kasper and S. M. Richards, Acta Cryst. 17, 752 (1964); R. H. Wentorf, Jr., and J. S. Kasper, Science 139, 338 (1963).
[48]A. S. Barker, Jr., Phys. Rev. 165, 917 (1968).
[49]J. C. Phillips, Phys. Rev. 104, 1263 (1956).
[50]G. F. Koster, in *Space Groups and Their Representations*, edited by F. Seitz and D. Turnbull (Academic, New York, 1957), p. 26.
[51]M. Cardona (private communication).
[52]P. B. Klein, H. Masui, Jin-Joo Song, and R. K. Chang, Solid State Commun. 14, 1163 (1974).
[53]The pressure coefficient of such a mode should have a large positive value because it is the difference of the positive TO and negative TA coefficients.
[54]R. Louden, J. Phys. (Paris) 26, 677 (1965).
[55]Since the Si sample was only 30 μm thick, this could not be a band-edge effect.
[56]R. J. Kobliska and S. A. Solin, Phys. Rev. Lett. 29, 725 (1972).
[57]H. Jex, Phys. Status Solidi (b) 45, 343 (1971).
[58]S. I. Novikova and N. Kh. Abrilkosov Fiz. Tverd. Tela [Sov. Physics-Solid State 5, 1558 (1964)]; R. H. Carr, R. D. McCammon, and G. K. White, Philos. Mag. 12, 157 (1965).
[59]This value is an average of the several results in the article by G. K. White (Ref. 3) and a recent measurement by R. K. Kirby and T. A. Hahn at NBS, which was supplied in a private communication.
[60]R. T. Payne, Phys. Rev. Lett. 13, 53 (1964).
[61]A. Bienenstock, Philos. Mag. 9, 755 (1964).
[62]J. F. Vetelino, S. S. Mitra, and K. V. Namjoshi, Phys. Rev. B 2, 967 (1970).
[63]W. Richter, J. B. Renucci, and M. Cardona, Solid State Commun. 16, 131 (1975).
[64]W. Weber, Phys. Rev. Lett. 33, 371 (1974).
[65]R. M. Martin, Phys. Rev. Lett. 21, 536 (1968); R. M. Martin, Phys. Rev. 186, 871 (1969).
[66]J. C. Phillips, in *Bonds and Bands in Semiconductors*, edited by A. M. Alper, J. L. Margrave, and A. S. Nowick (Academic, New York, 1973), p. 94.
[67]Only atmospheric-pressure (room-temperature) neutron data exist for InSb, but an approximate comparison is possible since the transition pressure for this material is relatively low, ~ 23 kbar [R. E. Hanneman, M. D. Banus, and H. C. Gatos, J. Phys. Chem. Solids 25, 293 (1964)].